ELSEVIER

Journal of Nuclear Materials 290–293 (2001) 131–134

journal of nuclear materials

www.elsevier.nl/locate/jnucmat

Non-destructive structural analysis of surface blistering by TEM and EELS in a reflection configuration

S. Muto [a,*], T. Matsui [b], T. Tanabe [a]

[a] *Center for Integrated Research in Science & Engineering, Nagoya University, Chikusa-ku, Nagoya 464-8603, Japan*
[b] *Graduate School of Engineering, Nagoya University, Chikusa-ku, Nagoya 464-8603, Japan*

Abstract

We present a non-destructive structural analysis of blistering on silicon surfaces heavily irradiated by D^+ and He^+ ions using grazing incidence electron microscopy and electron energy-loss spectroscopy. The images and their electron diffraction indicate that the blister wall consists of a mixture of amorphous and nano-crystalline silicon in the D^+ implanted sample, whereas the He^+ implanted blister shows an amorphous wall containing a high density of bubbles. The presented method enables us to delineate the cross-sectional view of the blister structure. The thickness of the top skin was found to be much less than the projected range of D^+ or He^+. The presented results suggest that surface diffusion is enhanced by the local stress concentration as well as a chemical effect.

Keywords: Electron microscopy; Electron energy loss spectroscopy; Blistering; Ion irradiation; Surface analysis

1. Introduction

Surface roughening of plasma facing materials by plasma (ion) irradiation very much influences plasma material interaction, though changes of sputtering, reflection and hydrogen retention. We have developed a new technique based on reflection electron microscopy (REM) [1], which makes it possible to analyze the structure of surface ridges and/or blisters on brittle materials non-destructively. Here we present the structural analysis of surface blistering on silicon wafers, produced by deuterium and helium ion bombardment.

2. Experimental

The sample was a commercial (1 0 0) silicon wafer, one side of which was electrochemically polished. The wafer was cut into rectangular parallelepiped blocks of 1 mm × 1 mm × 2 mm. Each block was mounted on a molybdenum single hole mesh with the shiny side edge-on to the center of the mesh. The shiny polished side of the sample was D^+ (deuteron)- or He^+-irradiated in a vacuum chamber ($\sim 5.0 \times 10^{-6}$ Pa) at room temperature with an accelerating voltage of 10 keV for D^+ and 16 keV for He^+ irradiation to give the nearly same projected range (~200 nm). The irradiated sample was then removed from the vacuum, exposed to air, and transferred into a transmission electron microscope (TEM), Jeol-JEM200CX, equipped with a parallel electron energy-loss spectrometer (EELS), Gatan Digi-PEELS model 766, in the conventional way. Observation and EELS measurements were conducted by grazing incidence electron microscopy (GIEM). The detailed experimental setup has already been described in [1].

3. Results

GIEM images of surface blistering are shown in Figs. 1(a)–(c) with the irradiated ion fluence inset in each. The blister size and density are much smaller for He^+ irradiation (He-blister) than those for D^+ irradiation

* Corresponding author. Tel.: +81-52 789 5200; fax: +81-52 789 5158.
E-mail address: muto@cirse.nagoya-u.ac.jp (S. Muto).

0022-3115/01/$ - see front matter
PII: S0022-3115(00)00556-0

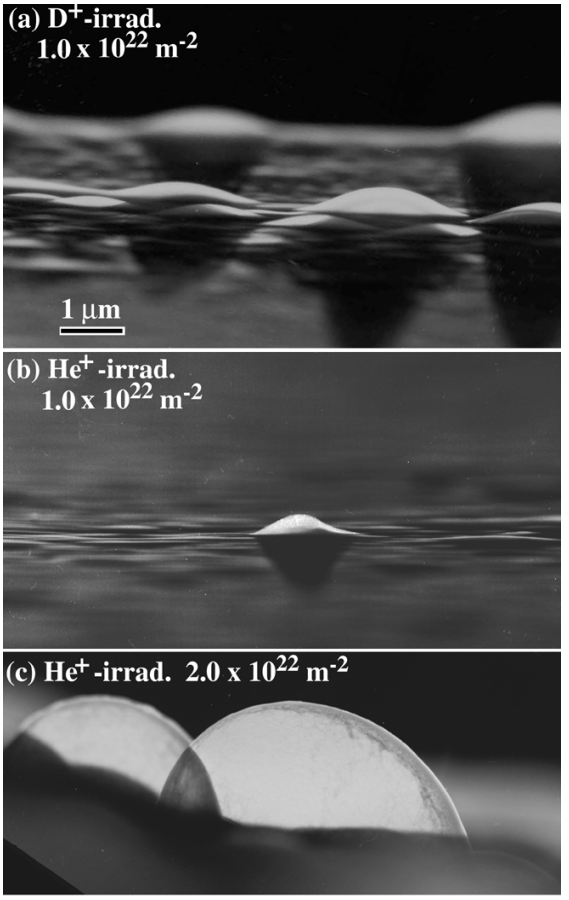

Fig. 1. GIEM images of blisters on silicon surface. Implant species and their fluence are inset.

(D-blister) at the same fluence, as shown in (a) and (b). This suggests that ion species chemically active with target materials are more effective for blistering because the implanted D atoms break the Si–Si bonds by formation of stronger Si–D bonding, which facilitates the crack propagation.

Enlarged images of an isolated blister are shown in Figs. 2(a) and (b) for D^+ and He^+ irradiation, respectively. The inset electron diffraction (ED) patterns were taken by inserting the selected area aperture diaphragm at the central part of each blister. The ED pattern in the D-blister: (a) is characterized by a superposition of sharp Debye–Scherrer rings and diffuse halo rings, whereas that in the He-blister, (b) shows only diffuse halo rings. The radii of the sharp rings were confirmed to be consistent with the lattice spacing of crystalline silicon. These indicate that the D-blister wall consists of a mixture of amorphous and fine granular polycrystalline silicon structures, whereas the He-blister wall is just an amorphous sponge-like structure containing a high density of small bubbles. The nano-crystalline particles

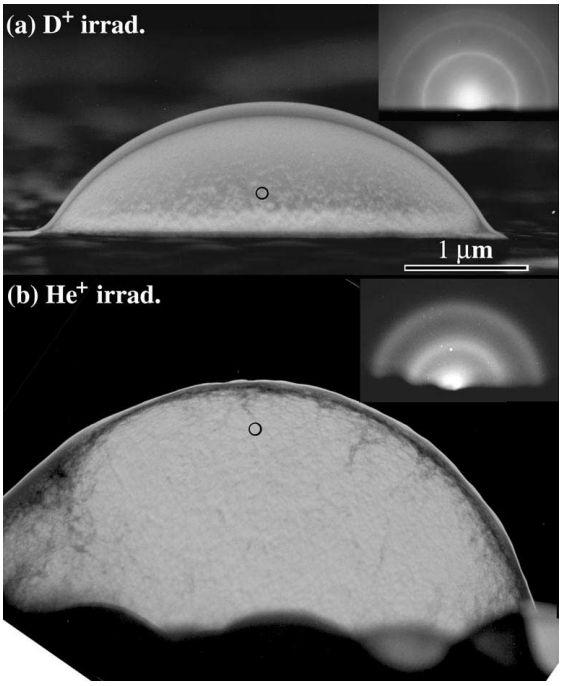

Fig. 2. Enlarged images and corresponding ED patterns of D-blister (fluence: 1.0×10^{22} m^{-2}) (a) and He-blister (fluence: 2.0×10^{22} m^{-2}) (b).

are considered to be formed by the significant local heat released by deuterium–deuterium recombination [2].

Representative EELS spectra in the plasmon-loss region obtained from the corresponding encircled areas of the blister walls in Fig. 2 are shown in Fig. 3. The spectra were acquired in the TEM image mode by placing the area of interest on the optical axis of the spectrometer. Considering the column approximation in

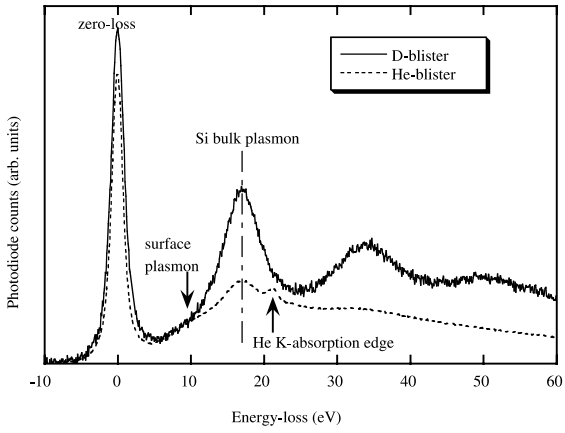

Fig. 3. EELS spectra acquired from the encircled areas in Fig. 2(a) and (b).

the high-energy electron diffraction theory (i.e., beam divergence inside the sample) [3] and the size of the small spectrometer collection aperture (~100 nm in diameter on the image) the obtained spectra come from the areas within the indicated circles. The He K-shell absorption edge is clearly seen in the He-blister, as shown in Fig. 3, which is unambiguous evidence of He incorporation inside the He-blister. On the other hand, core-loss of D was not detected with the preset energy-resolution (~1 eV).

The changes in the plasmon energy and the peak height ratio of bulk plasmon to zero-loss, I_p/I_0, obtained subsequently from the top of the D-blister wall to the bottom are shown in Figs. 4(a) and (b), respectively. It is seen that the plasmon energy is gradually shifted to the lower energy side with increasing distance from the top surface to the bottom. The plasmon energy of 23.8 eV at the top probably corresponds to that of SiO_2, indicating that the blister surface is highly oxidized. Hydrogenated silicon surfaces like porous silicon made by electropolishing in an HF solution are known to be very easily oxidized [4]. As the data acquisition position moves from top to bottom, the electron path-length becomes dominated by the silicon layer and the plasmon energy is shifted to the value of bulk silicon (~17 eV). The He-blister exhibits no such plasmon peak shift (not shown).

The specimen thickness, t, through which the incident electrons travel can be measured in general by the formula, $I_0 = I_t \exp(-t/\lambda)$, where I_0 is the zero-loss intensity, I_t is the total intensity reaching the spectrometer and λ is the electron mean free path for energy-loss. Since I_0 and I_t correlate with each other, the plot of I_p/I_0 in Fig. 4(b) reflects the effective thickness through which the incident electrons penetrate. One can thus estimate the path length of electrons through the sample, which enables us to delineate the cross-sectional view of the blister. The absolute values of the effective thickness were derived from a thickness vs. I_p/I_0 calibration plot for a crystalline silicon standard wedge-shape thin film.

The obtained cross-sectional view for D- and He-blisters is shown in Figs. 5(a) and (b). Note that the effective thickness of the blister wall is much less than the projected range (~200 nm) of D or He calculated with a Monte-Calro simulation code, TRIM92, and the skin thickness is not uniform over the entire blistering area.

Suppose that blistering occurs simply by implanted gas molecules accumulated around the projected range (~200 nm from the surface) extruding the surface layer by their pressure (gas-bubble network model) [5]. Since silicon has almost no ductility, a certain amount of silicon atoms in the surface layer should flow outward from the center of the blistering region to form the protruded wall, presumably by local stress concentration as a driving force. This would result in a thinner wall at the top of the blisters in agreement with the experimentally obtained structure, as shown in Fig. 5. One can

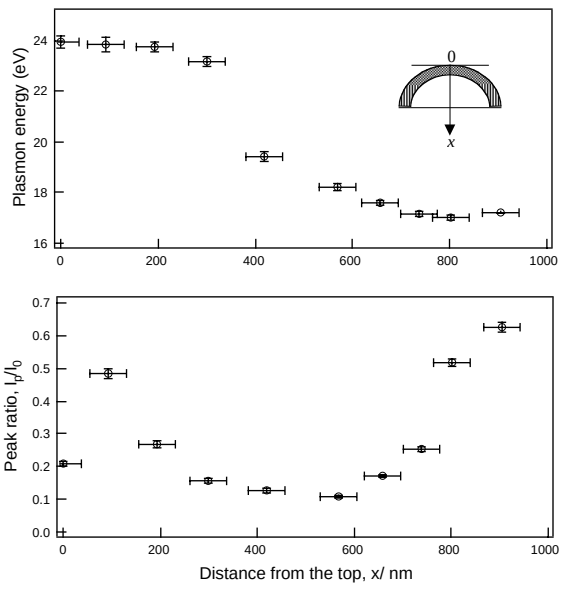

Fig. 4. (a) Bulk plasmon energy and (b) peak height ratio of bulk plasmon to zero-loss for the D-blister as a function of position, x, as shown inset in Fig. 2(a).

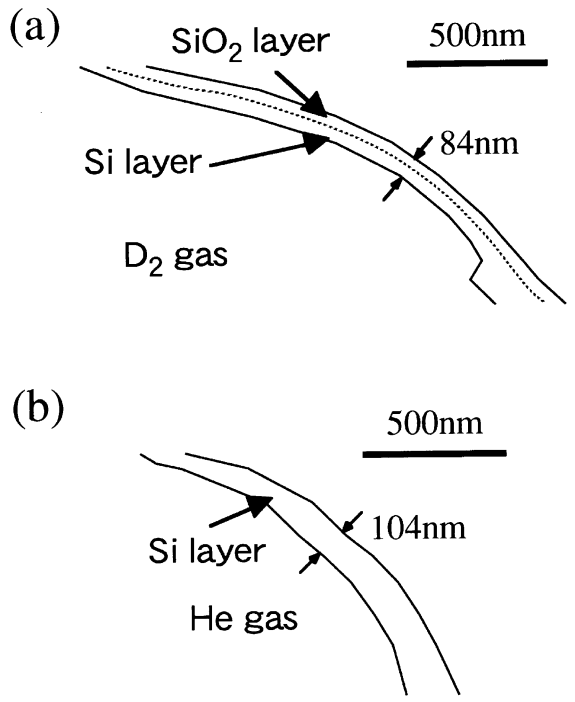

Fig. 5. Derived cross-sectional structures of D-blisters (a) and He-blisters (b).

Table 1
Experimental and calculated structural parameters for D- and He-blister

Blister type (fluence m^{-2})	Radius of curvature (nm)	Average height (nm)	Expected wall thickness (nm)	Experimental wall thickness (nm)	Number density ($\times 10^{10}/m^2$)	Gas volume density ($\times 10^{-8}/m^2$)
D-blister (1.0×10^{22})	2300	880	182	84	1.1	1.0
He-blister (2.0×10^{22})	1230	852	142	104	1.6	5.6

thus roughly estimate the expected average blister wall thickness by its curvature and height measured on the GIEM images. In Table 1 are tabulated the blister curvature, height, calculated average wall thickness, and the wall thickness obtained from the EELS measurement for both D- (fluence: 1.0×10^{22} m^{-2}) and He-blisters (fluence: 2.0×10^{22} m^{-2}). The wall thickness is still significantly smaller than the expected thickness, especially for D-blisters. The reason would be twofold: the surface atoms are considerably sputtered at such high fluence irradiation and, furthermore, D^+-irradiation especially leads to chemical sputtering.

In Table 1, the number density of the blisters and average gas volume density contained within the blisters are shown. The latter was estimated from the size and shape of the blisters in the GIEM images. Now let us try to derive the gas amount, n, inside the blisters. The average inside gas pressure, P, relates to the surface tension, γ, of the blister by the following relation:

$$\frac{4\gamma}{r} = P, \tag{1}$$

where r is the radius of the blister curvature, measured on the GIEM images. γ is roughly expressed by st, where s is the critical yield stress of silicon and t the blister wall thickness. This and Eq. (1) together with the equation of state of ideal gas lead to

$$n = \frac{4tV}{Rt}s, \tag{2}$$

where R is the gas constant and V is the internal volume within the blister. A precise value of s is not available but assuming that all the implanted He atoms are inside the blisters or bubbles, the critical yield stress, s, can be estimated from Eq. (2) and Table 1 to be $\sim$4 GPa. This value is reasonable because the bulk modulus, μ, of silicon is $\sim$100 GPa and the yield stress is supposed to be $\sim\mu/30$ according to a detailed calculation [6]. The total amount of D atoms per unit area within the D-blisters in the form of D_2 molecules can then be estimated to be $\sim 3 \times 10^{21}$ m^{-2}. This value is only $\sim$30% of the total implanted D atoms. This result suggests that most implanted D atoms are distributed within the Si matrix in the form of Si–D complexes.

4. Summary

We conducted a non-destructive structural analysis of blistering on silicon surfaces heavily irradiated by D^+ and He^+ ions using grazing incidence electron microscopy and electron energy-loss spectroscopy. The images and their electron diffraction indicate that the skin of the D-blister consists of a mixture of amorphous and nanocrystalline silicon, whereas the He^+ implanted blister shows an amorphous wall containing a high density of bubbles. Blistering occurs by the gas-bubble network model, in which D atoms breaking S–Si bonds act much more effectively for crack propagation than inert He atoms. The thickness of the blister wall was found to be much less than the projected range of D^+ and He^+, expected by a Monte-Carlo simulation, which is presumably due to physical and chemical sputtering and outward atomic flow driven by inhomogeneous stress concentration during the blistering process.

References

[1] S. Muto, T. Matsui, T. Tanabe, Jpn. J. Appl. Phys. 39(6A) (2000) (in printing).
[2] Q. Wang, G. Yue, J. Li, D. Han, Solid State Commun. 113 (2000) 175.
[3] P.B. Hirsch, A. Howie, R.B. Nicholson, D.W. Pashley, M.J. Whelan, Electron Microscopy of Thin Crystals, Krieger, New York, 1977 (Chapter 4).
[4] K. Furuya, M. Song, Y. Fukuda, T. Noda, T. Saito, J. Surf. Anal. 3 (1997) 233.
[5] T. Katabuchi, N. Kawachi, Y. Tagishi, J. Appl. Phys. 86 (1999) 3030.
[6] J. Weertman, J.R. Weertman, Elementary Dislocation Theory, Macmillan, New York, 1964 (Chapter 1).